Soils and Rocks

www.soilsandrocks.com

An International Journal of Geotechnical and Geoenvironmental Engineering

ISSN 1980-9743
ISSN-e 2675-5475

Numerical simulation of responses of a grid-shaped soil improvement foundation (TNF) on silty ground subjected to consecutive earthquakes

Han Vo-Cong[1#], Kinji Takeuchi[2], Yasuo Tomono[1], Tatsunori Matsumoto[3]

Case Study

Keywords
TNF
Liquefaction
Settlement
Silty ground
Finite element method (FEM)

Abstract

Liquefaction induced by earthquakes causes instability of buildings such as large average and/or relative settlements. Such occurrences can lead to damage to the building structures. Usually, when an earthquake occurs, saturated loose sandy ground is the most susceptible to liquefaction. Even for saturated silty ground with small SPT *N*-values, the possibility of liquefaction needs to be considered in the design process of the foundation. Tender Net Foundation (TNF) is a kind of shallow foundation with a combination of grid-shaped soil improvement to depths of 2 to 3 meters, concrete slab, and concrete single footings. In this paper, the dynamic analysis of an actual TNF on the silty ground subjected to three consecutive earthquakes was conducted. Measurements of the settlements of the TNF were initiated after the second earthquake. The silty ground was modeled by the UBC3D-PLM model. The ground accelerations recorded about 10 km away from the site area were used as the input accelerations in the dynamic analyses. The responses of the TNF as well as the ground during and after the earthquakes were analyzed. The numerical analyses simulated the measured settlements well. Furthermore, a comparison was conducted between the TNF and the conventional shallow foundation to demonstrate the advantages of the TNF in reducing the average and differential settlements.

1. Introduction

Tender Net Foundation (TNF) (Takeuchi Construction Inc., 2025) is a kind of shallow foundation with a combination of grid-shaped soil improvement (primary soil improvement), a flat soil improvement on the primary soil improvement (secondary soil improvement), concrete slab and concrete single footings (see Figures 1 and 2). The original soil is improved by blending with cement as a solidification material using a backhoe. Cement powder with lower elution of hexad chrome is mixed with the original soil at the site for environmental friendliness. The mass of cement per unit soil volume is varied so that the improved soil has an unconfined compression strength q_u of 300 to 450 kPa in common. Han Vo Cong et al. (2022) analyzed the TNF system subjected to vertical loading and demonstrated that the TNF system is an efficient foundation for reducing settlement and volume of soil improvement compared to the conventional shallow soil improvement method.

By improving the surface layer to depths of 2 to 3 meters in a grid shape, the TNF could be an efficient foundation for suppressing the damage to buildings when liquefaction occurs in the ground under the TNF.

In this paper, the dynamic analysis of a TNF for a one-story factory building on silty ground subjected to three consecutive earthquakes is conducted. Measurements of the settlements of the TNF were initiated one week after the second earthquake. The construction of the building was not completed at the first earthquake.

PLAXIS 3D FEM software (Bentley, 2022) was used for simulation analysis. The silty ground was modeled by the UBC3D-PLM model. The time histories of ground accelerations of three earthquakes recorded about 10 km away from the site area were used as the input accelerations in the dynamic analyses of the TNF. The responses of the TNF as well as the ground during and after the earthquakes were calculated. The calculation simulated the measured settlements well. The analysis showed that liquefaction occurs in the silty ground. To demonstrate the

[#]Corresponding author. E-mail address: han@takeuchi-const.co.jp
[1]Takeuchi Construction Inc., Research and Development Division, Mihara, Hiroshima, Japan.
[2]Takeuchi Construction Inc., Mihara, Hiroshima, Japan.
[3]Kanazawa University, Kanazawa, Ishikawa, Japan.

Submitted on January 28, 2025; Final Acceptance on July 30, 2025; Discussion open until February 28, 2026.

Editor: Renato P. Cunha

https://doi.org/10.28927/SR.2025.001525

advantages of the TNF for suppressing the settlements induced by liquefaction, a similar analysis of a conventional shallow foundation was also carried out for comparison purposes.

2. Outline of building and ground

Figure 3 shows the plan view of the construction site and two boreholes (BHs). The target of this analysis is a TNF for the foundation of a factory constructed in Fukushima, Japan. The factory is a one-story building with a floor dimension of 30 m × 19.5 m and a height of 5.7 m.

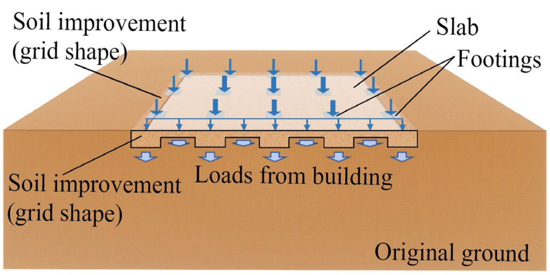

Figure 1. Section view of a TNF system.

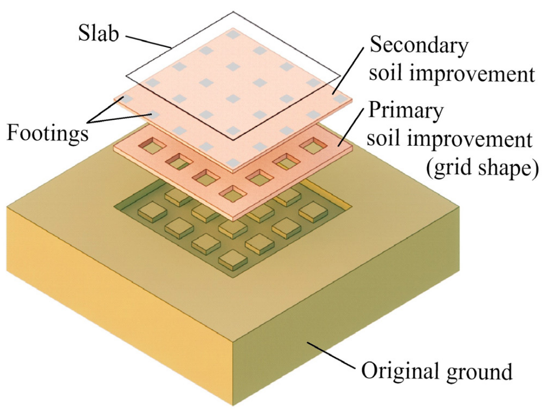

Figure 2. Composition of a TNF system.

Figure 4 shows the profiles of the soil layers and the SPT *N*-values. The ground at each borehole consists of 7 soil layers. The sandy silt layer 2 ($N = 1$) exists at depths 0.65 to 2.85 m (2.2 m thick) at BH No. 1, and at depths 1.19 to 3.09 m (1.9 m thick) at BH No. 2. The silt layer 4 ($N = 0 \sim 1$) exists at depths 3.85 to 13.65 m (9.8 m thick) at BH No. 1, and at 3.89 to 14.79 m (10.9 m thick) at BH No. 2. The groundwater level is 1.05 m at BH No. 1 and 1.19 m at BH No. 2 below the ground surface. Soil tests were conducted on the soil specimens of silt layers 2 and 4 at only BH No.1.

Figure 5 shows the plan view of the TNF system used for the foundation of the factory building. The size of the TNF system is 33.8 m × 25.6 m having a primary soil improvement layer with a thickness of 1.5 m, and a secondary soil improvement layer with a thickness of 0.8 m. The thickness of the concrete footings is 0.4 m and the thickness of the concrete slab is 0.2 m.

3. History of earthquakes and settlement measurements

Figure 6 shows the construction progress, earthquake history, and measured settlements at the five points of the TNF (see Figure 5). The first severe earthquake (EQ) with Japan Meteorological Agency (JMA, 2023) Seismic Intensity scale (*SI* scale) of 5- (5 lower) occurred on 2016-11-22, about 3 months after the completion of the TNF and just before the completion of the building on 2016-11-29. The settlements were zero at the completion of the TNF. The second severe EQ with *SI* scale of 5- occurred on 2017-02-28. The settlement measurements were initiated on 2017-03-07, one week after the second severe EQ. Several moderate EQs with *SI* scale of 4 occurred after the second severe EQ, and the third severe EQ with *SI* scale of 6- occurred on 2021-02-13. The settlement measurements were made on 2021-05-20. Interestingly, large ground settlements were measured after the occurrence of earthquakes having *SI* scale of 5- or higher. For example, an earthquake with *SI* scale of 5- is one in which many people are frightened and feel the need to hold onto something stable.

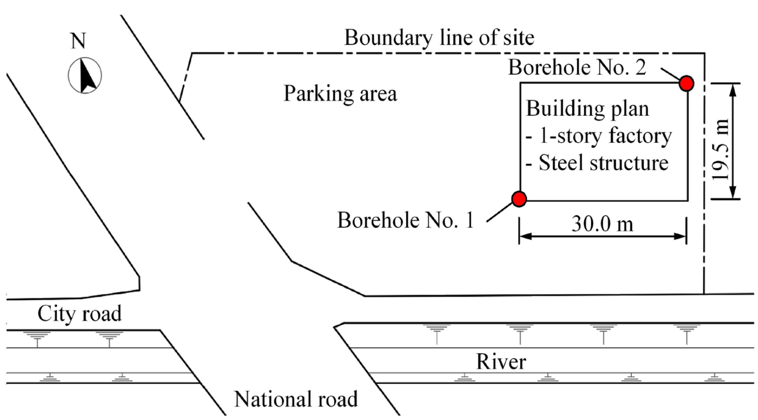

Figure 3. Plan view of the construction site and boreholes.

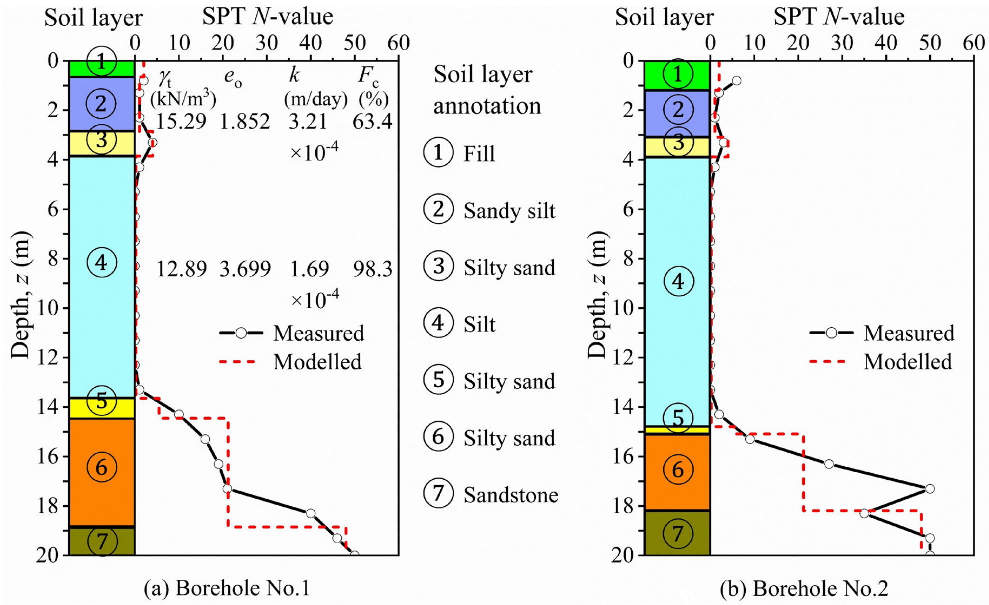

Figure 4. Profiles of soil layers and SPT *N*-values.

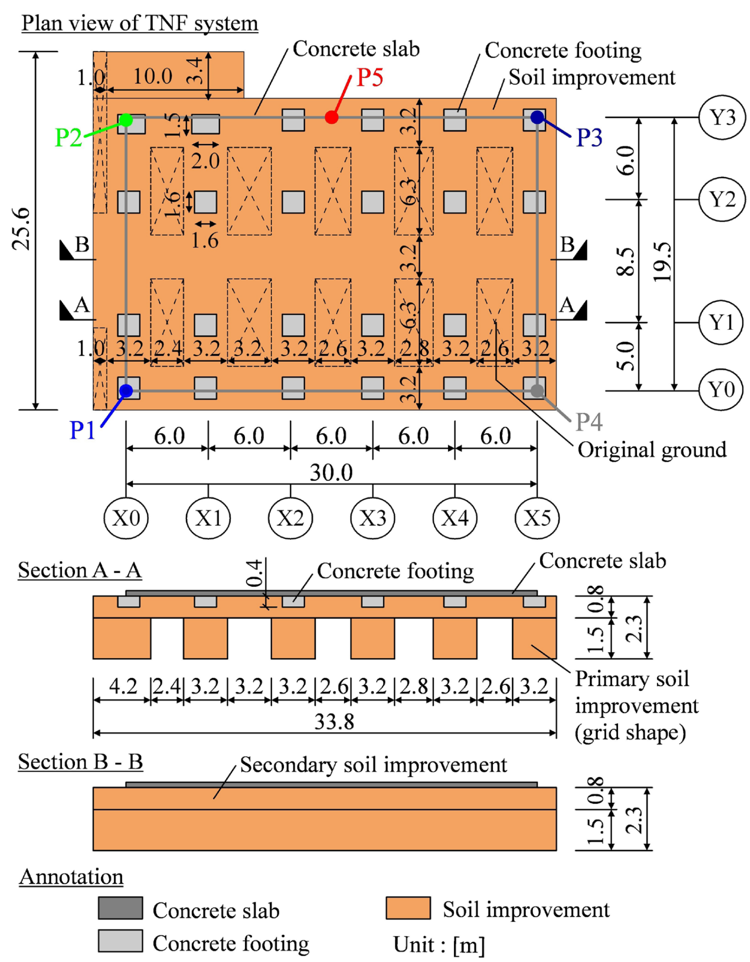

Figure 5. Plan view of the TNF system.

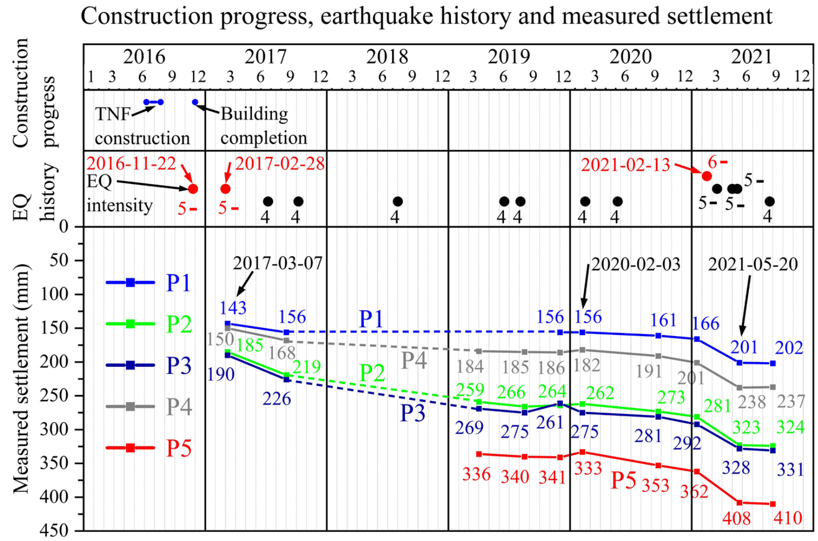

Figure 6. Construction progress, earthquake history, and measured settlements.

Hanging objects such as lamps swing violently. Dishes in cupboards and items on bookshelves may fall. Small cracks may form and liquefaction may occur in the ground. Refer to JMA (2023) for more details on *SI* scales.

Figure 7 shows the distributions of relative settlements of the TNF measured on 2017-03-07, on 2020-02-03 and on 2021-05-20 (98 days, 1161 days and 1633 days after the building completion), respectively. Measurements of the settlements of the TNF on 2017-03-07 were made at the four corners of the building. Those on 2020-02-03 were made at each position of the columns of the building. Those on 2021-05-20 were made at the periphery of the building. The measured relative settlements Δw were defined as the difference between the settlement at given points and the settlement at point P1 (X0, Y0).

It is seen that the maximum value of Δw and the average settlement w_{ave} on 2021-05-20 increased compared with those on 2020-02-03. That is, the maximum value of Δw was 186 mm and settlement at the reference point P1 was 156 mm in Figure 7b. Those were 207 mm and 201 mm in Figure 7c. Hence, the influence of earthquakes is strongly suspected as the cause of the differential settlement.

To investigate the cause of settlements of the TNF, the dynamic FEM analysis is conducted in this research.

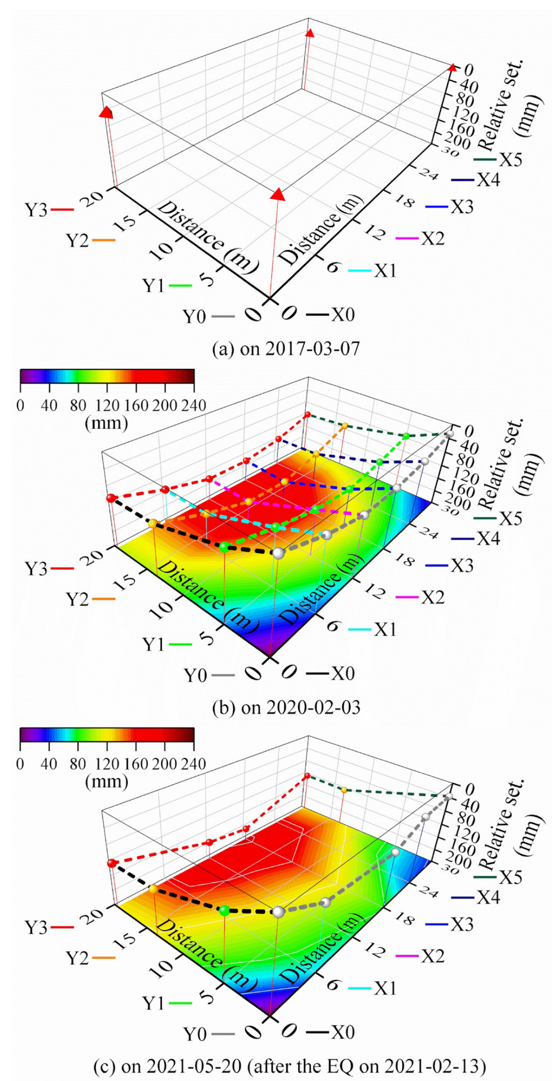

Figure 7. Distribution of measured relative settlements of the TNF.

4. Dynamic FEM analysis

4.1 Analysis conditions

Figure 8 shows the PLAXIS 3D FEM analysis model. The ground was modeled by 7 soil layers. The thickness of fill layer ① is 0.65 m at BH No.1 and 1.19 m at BH No.2. The dead loads of the building were applied as the point loads on the footings and the live load was applied as the uniform surface load of 3 kPa on the slab. The earthquake loads (accelerations) were applied to the bottom of the ground.

Figure 9 shows the analysis phases. The analysis phases were set following the construction progress and earthquake history. In this research, earthquakes with seismic intensity scale *SI* of 5- or higher on 2016-11-22 (1st EQ, *SI* = 5-), on 2017-02-28 (2nd EQ, *SI* = 5-), and on 2021-02-13 (3rd EQ, *SI* = 6-) were considered. The seven earthquakes with *SI* of 4 between 2017-02-28 and 2021-02-13 were omitted in this particular analysis because the settlements caused by these earthquakes were considered negligible. The ground accelerations of the earthquakes recorded about 10 km away from the site area were used as input accelerations of the three earthquakes in the dynamic analyses at Phases 3, 5 and 6. Free-field conditions were set at the outer side surfaces of the ground model. Undrained conditions were set for the ground below the groundwater level, while drained conditions were set for the ground above the groundwater level.

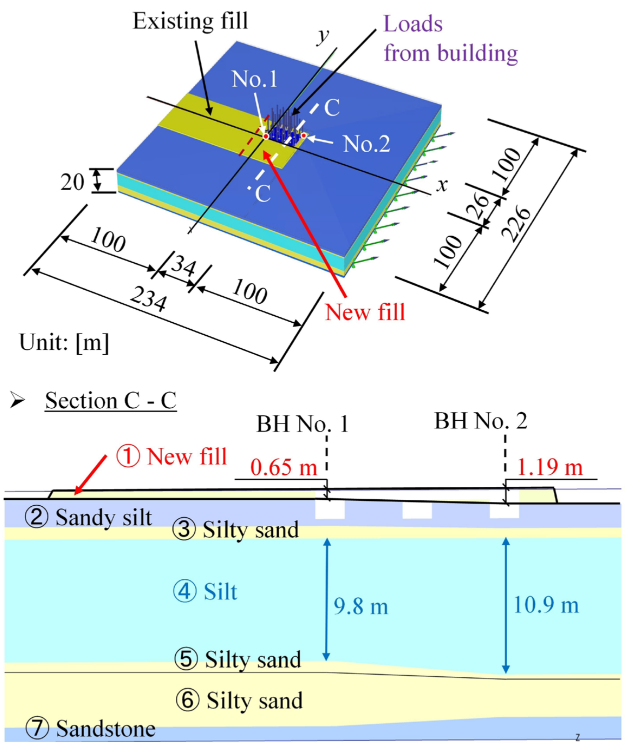

Figure 8. PLAXIS 3D FEM analysis model.

In the other phases, consolidation phenomena were considered. Horizontal displacements of the outer side surfaces of the ground model were fixed in the consolidation analyses.

Figure 10 shows the input acceleration data used in the dynamic analyses. The acceleration data were obtained from K-NET strong-motion seismograph network (Kyoshin Network, 2022) and were converted to acceleration data into *x*- and *y*-directions.

Table 1 shows the physical and mechanical properties of each soil layer. The thicknesses of soil layers, t_1 (in Borehole No. 1) and t_2 (in Borehole No. 2), along with the SPT *N* value for each soil layer, were determined based on the soil test results (see Figure 4). The wet unit weight γ_t, initial void ratio e_0 and coefficient of permeability *k* of the sandy silt layer ② and the silt layer ④ were obtained from soil test results (see Figure 4), while the corresponding properties for the other soil layers were assumed to be typical value of each soil type. In this analysis, the silt, sandy silt and silty sand layers (soil layers ②, ③, ④, ⑤ and ⑥) were modeled using the UBC3D-PLM model, while the other soil layers (soil layers ① and ⑦) were modeled using the linear elastic model.

Some rigorous constitutive models for liquefaction have been proposed, *ie*. SANISAND by Dafalias & Manzari (2004), t_{ij} model by Nakai et al. (2011) and so on. However, these models typically require a wide range of advanced laboratory test results to accurately determine input parameters. In this project, only SPT *N*-values were available, along with limited basic soil test data conducted on the silt layers ② and ④

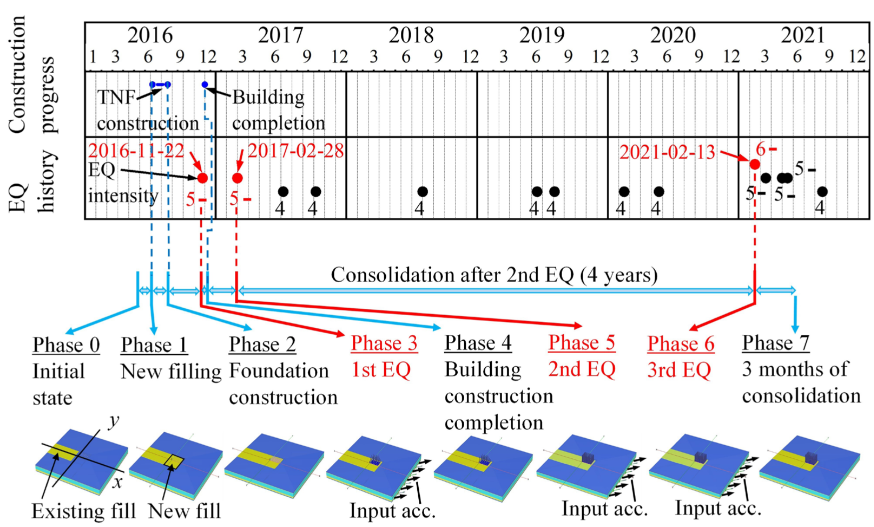

Figure 9. Analysis phases.

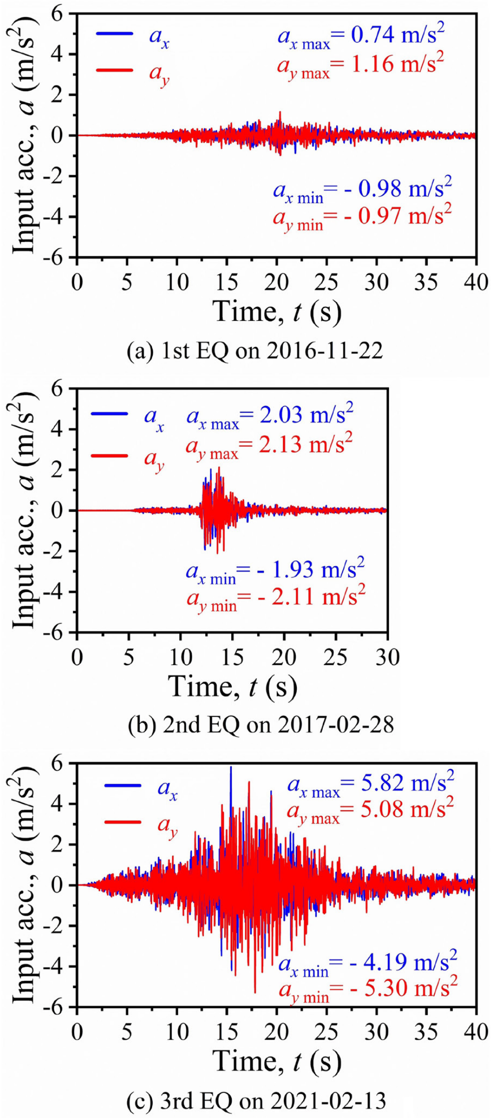

Figure 10. Input acceleration data.

at borehole BH No.1. The available data were not enough to use more complex models. Therefore, a more practical approach was adopted using the UBC3D-PLM model, which allows input parameters to be empirically estimated based on SPT N-values and basic soil properties.

Table 2 shows the parameters of the linear elastic model applied to soil layers ① and ⑦.

The SPT N-value in each layer was used for estimating shear wave velocity V_s using Equation 1 specified in Japan Road Association (2012).

$$V_s \text{ (m/s)} = \begin{cases} 100N^{1/3} & \text{for clay} \\ 80N^{1/3} & \text{for sand} \end{cases} \tag{1}$$

Shear modulus G was calculated using Equation 2, in which g is the gravitational acceleration (g = 9.8 m/s^2).

$$G = \frac{\gamma_t}{g} V_s^2 \tag{2}$$

Young's modulus E was calculated using Equation 3. In Equation 3, Poisson's ratio v of each soil layer was assumed as shown in Table 2.

$$E = 2(1+\nu)G \tag{3}$$

Table 3 shows the parameters of the UBC3D-PLM model applied to soil layers ②, ③, ④, ⑤ and ⑥.

The relative density D_r was estimated by means of Equation 4, as proposed in Tokimatsu & Yoshimi (1983). In Equation 4, σ_v' is the effective vertical stress in kgf/cm^2 (equivalent to 98 kPa). ΔN_f is the increment of the N-value based on the fine grain content rate F_c specified in The Building Center of Japan (2019). The F_c values of the sandy silt layer ② and the silt layer ④ were obtained from soil test results (see Figure 4), while the F_c values of the other soil layers were assumed to be 10%, 15% and 5% for layers ③, ⑤ and ⑥, respectively.

$$D_r = 21\sqrt{\frac{N}{\sigma_v' + 0.7} + \frac{\Delta N_f}{1.7}} \ (\%) \tag{4}$$

The constant volume friction angle ϕ_{cv} was calculated using Equation 5, as specified in Japan Road Association (2012). In Equation 5, σ_v' is the effective vertical stress in kPa.

$$\phi_{cv} = 4.8 \ln\left(\frac{170N}{\sigma_v' + 70}\right) + 21 \ (^\circ) \tag{5}$$

The peak friction angle ϕ_p was calculated using Equation 6 following PLAXIS 3D Manuals (Bentley, 2022).

$$\phi_p = \phi_{cv} + \frac{(N_1)_{60}}{10} + \max\left(0; \frac{(N_1)_{60} - 15}{5}\right) \ (^\circ) \tag{6}$$

The corrected SPT value $(N_1)_{60}$ was calculated using Equation 7 following PLAXIS 3D Manuals (Bentley, 2022).

$$(N_1)_{60} = \frac{D_r^2}{15^2} \tag{7}$$

The cohesion c of all soil layers was assumed to be 0. The other parameters of the UBC3D-PLM model, as listed in Table 3, were either calculated or set following PLAXIS 3D Manuals (Bentley, 2022).

Table 4 shows the material parameters of concrete and soil improvement used for the TNF system. The parameters of the soil improvement of the TNF were estimated using Equations 1, 2 and 3 assuming an N-value of 20 and γ_t of 17 kN/m^3.

4.2 Analysis results

Figure 11 shows the calculated settlement curves of the TNF at five points. Large settlements occurred during each earthquake. Settlements were largest in the 3rd EQ with SI = 6-. It is seen that the earthquakes also caused differential settlements of the TNF.

The analysis of a case of no earthquake was also conducted to evaluate the influence of the earthquakes. The calculated settlement curve at point P5 of this case is added in Figure 11. It is seen that the earthquakes were the main cause of large settlements of the TNF.

Figure 12 shows the effective vertical stress $'_{v}$ during the 1st EQ. The σ'_v of all soil layers of the ground decreased during the earthquake. At the end of the 1st EQ, the σ'_v of silty ground (layers ② and ④) and sandy ground (layer ③)

Table 1. Physical and mechanical properties of each soil layer.

Layer No.	Soil type	Soil model	t_1 (m)	t_2 (m)	SPT N	γ_t (kN/m^3)	e_0	k (m/day)
①	Fill	Linear elastic	0.65	1.19	2	17.00	1.0	8.64
②	Sandy silt	UBC3D-PLM	2.20	1.90	1	15.29	1.852	3.21×10^{-4}
③	Silty sand	UBC3D-PLM	1.00	0.80	4	17.00	0.9	8.64×10^{-3}
④	Silt	UBC3D-PLM	9.80	10.90	0~1	12.89	3.699	1.69×10^{-4}
⑤	Silty sand	UBC3D-PLM	0.80	0.30	5.5	17.00	0.9	8.64×10^{-3}
⑥	Silty sand	UBC3D-PLM	4.40	3.10	21.2	17.00	0.8	8.64×10^{-3}
⑦	Sandstone	Linear elastic	1.15	1.81	48	20.00	0.5	0

Legend: see List of symbols and abbreviations.

Table 2. Parameters of the linear elastic model applied to soil layers ① and ⑦.

Layer No.	Soil type	Soil model	SPT N	γ_t (kN/m^3)	V_s (m/s)	G (kPa)	v	E (kPa)
①	Fill	Linear elastic	2	17.00	100.8	1.76×10^4	0.3	4.58×10^4
⑦	Sandstone	Linear elastic	48	20.00	363.4	26.95×10^4	0.2	64.69×10^4

Legend: see List of symbols and abbreviations.

Table 3. Parameters of the UBC3D-PLM model applied to soil layers ②, ③, ④, ⑤ and ⑥.

Layer No.	D_r (%)	ϕ_{cv} (°)	ϕ_p (°)	$(N_1)_{60}$	c (kPa)	k_B^e	k_G^e	k_G^p	R_f	m_e	n_e	n_P	σ_t (kPa)	f_{dens}	f_{Epost}
②	59.7	22.7	24.4	15.8	0	763	1090	920	0.73	0.5	0.5	0.4	0	1.0	1.0
③	54.1	29.3	30.6	13.0	0	714	1021	618	0.75	0.5	0.5	0.4	0	1.0	1.0
④	64.5	22.7	25.2	18.5	0	803	1148	1277	0.71	0.5	0.5	0.4	0	1.0	1.0
⑤	62.8	30.3	32.6	17.5	0	789	1127	1139	0.72	0.5	0.5	0.4	0	1.0	1.0
⑥	67.2	36.2	39.2	20.1	0	826	1179	1525	0.70	0.5	0.5	0.4	0	1.0	1.0

Legend: see List of symbols and abbreviations.

Table 4. Material parameters of concrete and soil improvement used for the TNF system.

Material	Soil model	γ_t (kN/m^3)	V_s (m/s)	G (kPa)	v	E (kPa)
Concrete (Slab, Footing)	Linear elastic	24	2001	9.79×10^6	0.2	23.50×10^6
Soil improvement	Linear elastic	17	271	1.28×10^5	0.25	3.20×10^5

Legend: see List of symbols and abbreviations.

decreased to nearly 0 kPa. It is seen that liquefaction occurs even in the silty ground.

Figure 13 shows the excess pore water pressure p_{excess} during the 1st EQ. The p_{excess} of the whole ground increased during the earthquake, and the p_{excess} at the end of the 1st EQ was much larger than those before the earthquake, especially in silty ground (layers ② and ④). The p_{excess} at the end of the 1st EQ caused consolidation settlements of the TNF and the surrounding ground after the earthquake as shown in Figure 11.

Figure 14 compares the calculated settlements and the measured settlements of the TNF on 2017-03-07, 2020-02-03 and 2021-05-20, respectively. As shown in Figure 14a, the calculated settlements closely match the measured settlements at the four corners of the foundation (at the measurement points). As shown in Figure 14b, although the calculated settlements are smaller than the measured settlements, the distributions of calculated settlements align well with the distributions of measured settlements. In Figure 14c, although the number of measurement points is less, the trend of the distribution of the calculated results remain consistent with that of the measured results.

Figure 15 compares the calculated relative settlements and the measured relative settlements of the TNF on 2017-03-07, 2020-02-03 and 2021-05-20, respectively. In Figure 15a, comparing the distribution of relative settlements is difficult due to the measured settlement data are only available at the four

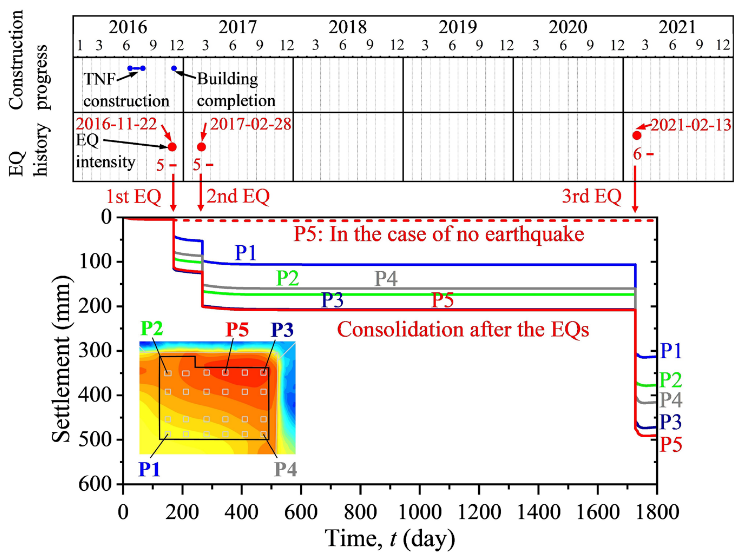

Figure 11. Calculated settlement curves of the TNF.

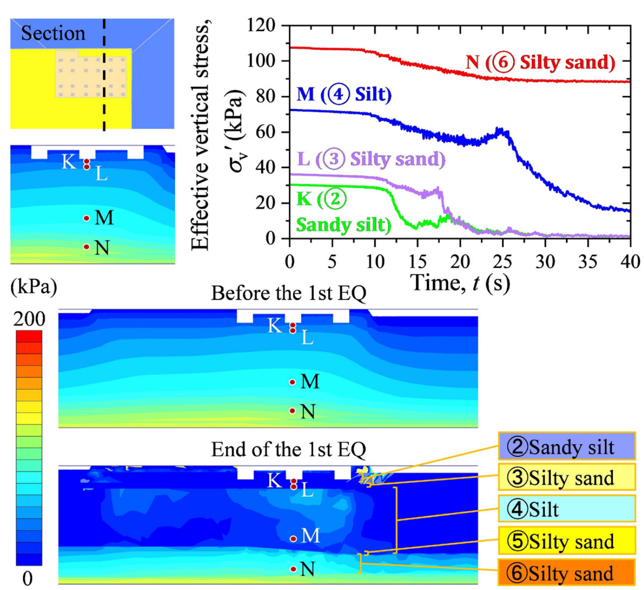

Figure 12. Effective vertical stress during the 1st EQ.

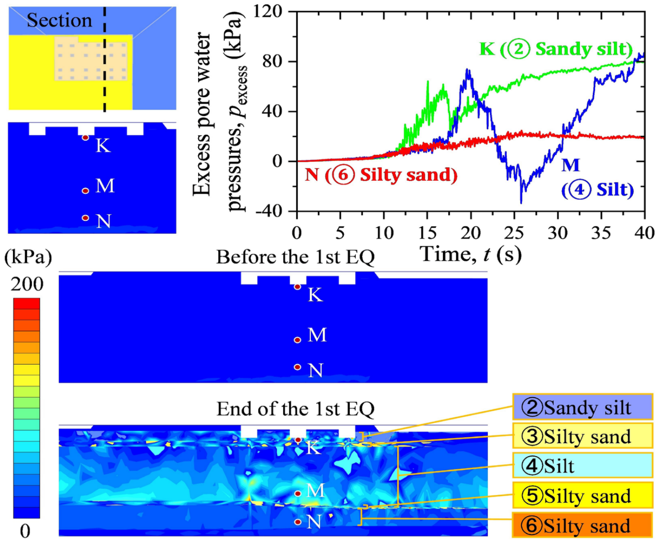

Figure 13. Excess pore water pressure during the 1st EQ.

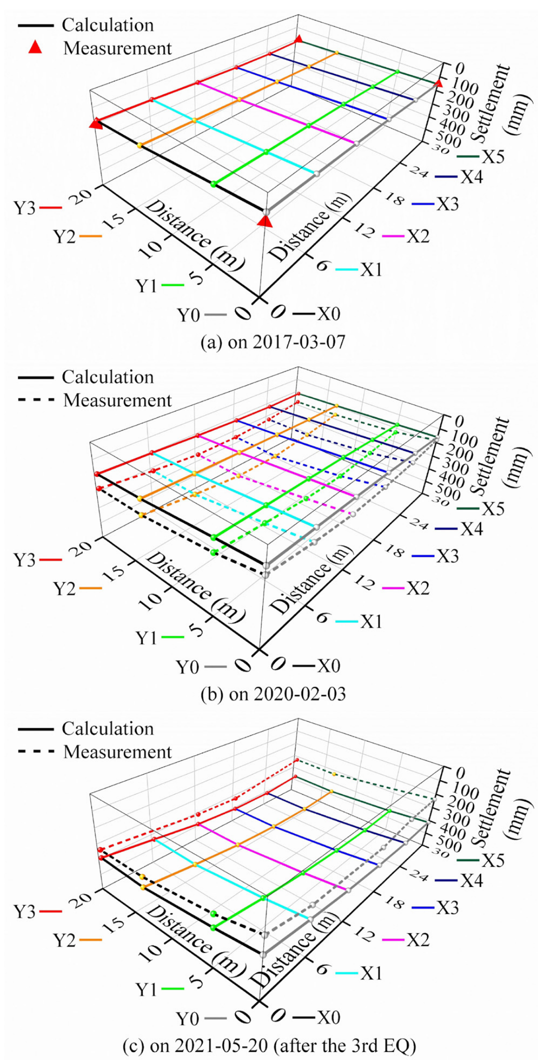

Figure 14. Comparison of calculated and measured settlements of the TNF.

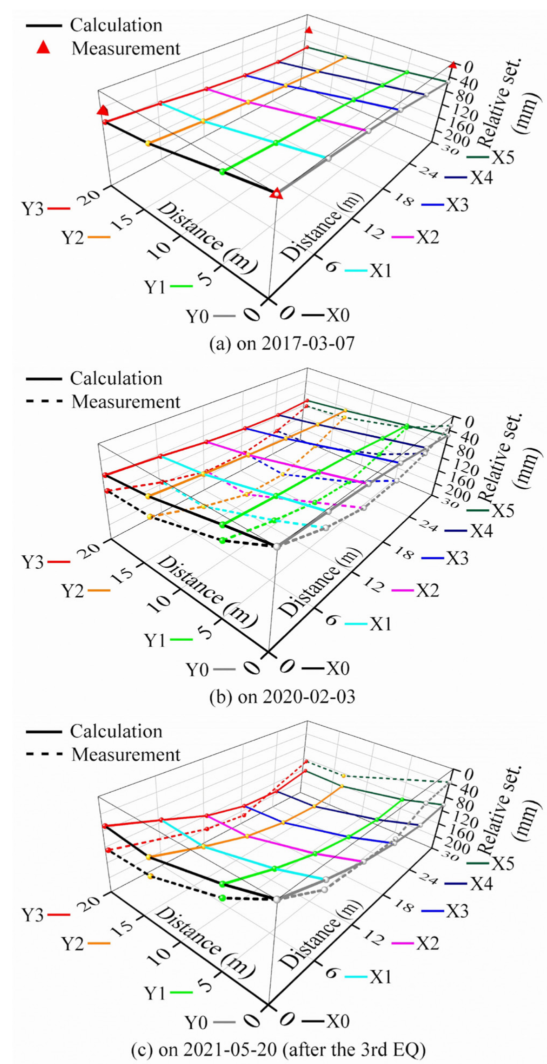

Figure 15. Comparison of calculated and measured relative settlements of the TNF.

corners of the foundation. However, in Figures 15b and 15c, the distributions of relative settlements in the measurement and the calculation are nearly the same. Hence, the calculation simulated well the measured settlements.

Figure 16 shows the comparison of the calculated and measured relative settlements on 2021-05-20 (after the 3rd EQ). It is seen that the calculation simulated the measured settlements well. Along the Y-axis direction (Figure 16a), the maximum settlement occurred at the center points (X3 axis) in both the measurement and the calculation, and the settlement gradually decreased toward the edges. Along the X-axis direction (Figure 16b), the calculated maximum settlements occurred between at the Y2 axis and Y3 axis. Along X0 axis and X5 axis, similar results were measured. Although there were only two measurement points along the X3 axis, it is inferred that a similar trend occurred.

To demonstrate the efficient performance of the TNF for suppressing the settlements induced by liquefaction, a similar analysis of a conventional shallow foundation shown in Figure 17 was conducted.

Figure 18 shows the comparison of the calculated settlement curves at point P5 between the TNF and the conventional shallow foundation. It is seen that the settlement of the TNF is suppressed compared to the settlement of the conventional shallow foundation, especially in the 3rd EQ (*SI* = 6-).

Figure 19 shows the comparison of the distribution of calculated relative settlements between the TNF system and the conventional shallow foundation on 2021-05-20 (after the 3rd EQ). It is seen that the differential settlement in the case of the TNF is much suppressed compared to the conventional shallow foundation. This demonstrates the advantages of the TNF for suppressing the settlements induced by liquefaction, highlighting its advantages over conventional foundation methods.

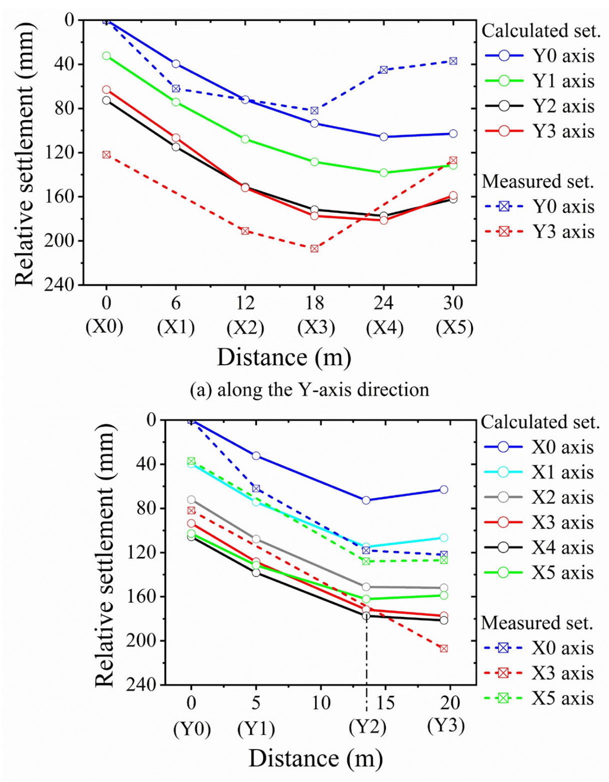

Figure 16. Comparison of calculated settlements and measured settlements on 2021-05-20 (after the 3rd EQ).

Figure 17. Section view of a conventional shallow foundation.

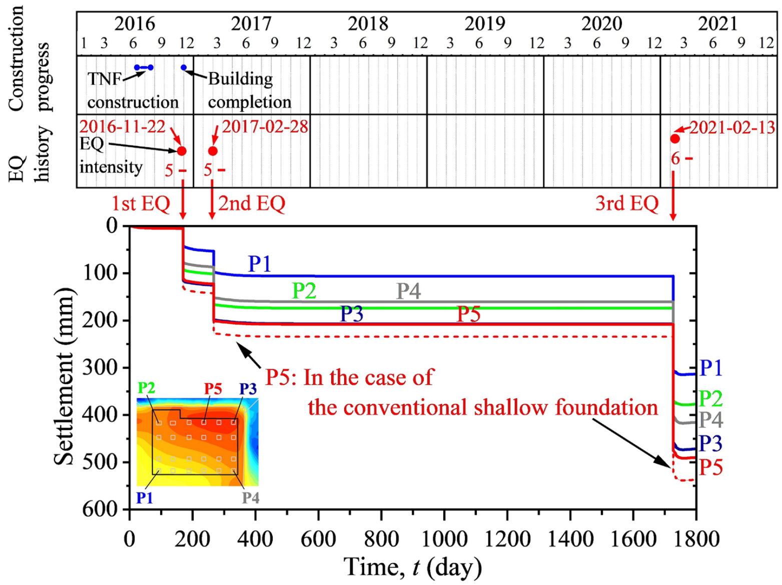

Figure 18. Comparison of calculated settlement curves between the TNF and the conventional shallow foundation.

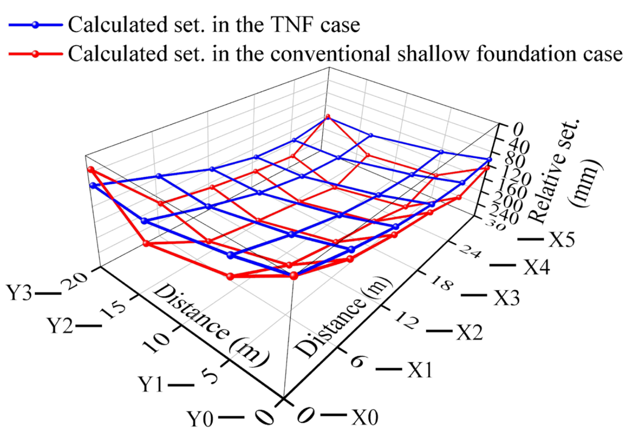

Figure 19. Comparison of the distribution of calculated relative settlements between the TNF system and the conventional shallow foundation on 2021-05-20 (after the 3rd EQ).

5. Conclusions

In this research, the dynamic analysis of the actual TNF on the silty ground subjected to three consecutive earthquakes was conducted. The responses of the TNF as well as the ground during and after the earthquakes were calculated to investigate the occurrence of liquefaction in the silty ground. Comparisons of the calculated settlements and the measured settlements after the second and third earthquakes were conducted. An analysis of a case of no earthquake was also conducted to investigate the influence of the earthquakes. Furthermore, a similar dynamic analysis of a conventional shallow foundation was also carried out to compare its performance in suppressing the settlements induced by liquefaction with the TNF's performance. From comparisons between the measured and calculated results, the main conclusions are drawn as follows:

1. The dynamic calculation of the TNF simulated the measured settlements well;
2. Earthquakes were the main cause of settlements and differential settlements of the TNF in this project, because settlements of the TNF from the analysis of the case of no earthquake were much less than those caused by the earthquakes;
3. Liquefaction occurred even in the silty ground;
4. The TNF is a more efficient foundation for suppressing the settlements induced by liquefaction compared to the conventional shallow foundation.

In the next step, a sensitivity analysis would be needed to investigate the influences of soil parameters on settlement results, enhancing the practical value of this research.

Declaration of interest

The authors have no conflicts of interest to declare. All co-authors have observed and affirmed the contents of the paper and there is no financial interest to report.

Authors' contributions

Han Vo-Cong: formal analysis, methodology, visualization, writing – original draft. Kinji Takeuchi: conceptualization, resources. Yasuo Tomono: project administration, supervision, investigation. Tatsunori Matsumoto: conceptualization, supervision, validation.

Data availability

No dataset was generated or evaluated in the course of the current study; therefore, data sharing is not applicable.

Declaration of use of generative artificial intelligence

This work was prepared without the assistance of generative artificial intelligence (GenAI) tools.

List of symbols and abbreviations

a_x	Acceleration into x-direction
a_y	Acceleration into y-direction
c	Cohesion
e_0	Initial void ratio
f_{dens}	Densification factor
f_{Epost}	Post-liquefaction factor
g	Gravitational acceleration
k	Coefficient of permeability
$k_B{}^e$	Elastic bulk modulus factor
$k_G{}^e$	Elastic shear modulus factor
$k_G{}^p$	Plastic shear modulus factor
m_e	Rate of stress-dependency of elastic bulk modulus
n_e	Rate of stress-dependency of elastic shear modulus
n_p	Rate of stress-dependency of plastic shear modulus
p_{excess}	Excess pore water pressure
q_u	Unconfined compression strength
t_1	Thickness of soil layer in Borehole No. 1
t_2	Thickness of soil layer in Borehole No. 2
w_{ave}	Average settlement
BH	Borehole
D_r	Relative density
E	Young's modulus
EQ	Earthquake
F_c	Fine grain content rate
FEM	Finite Element Method
G	Shear modulus
JMA	Japan Meteorological Agency
$(N_1)_{60}$	Corrected SPT value
R_f	Failure ratio
SI	Seismic Intensity scale
SPT	Standard Penetration Test
TNF	Tender Net Foundation
V_s	Shear wave velocity
γ_t	Wet unit weight
ν	Poisson's ratio
σ_t	Tension cut-off
$\sigma_v^{'}$	Effective vertical stress
ϕ_{cv}	Constant volume friction angle
ϕ_p	Peak friction angle
ΔN_f	Increment of the N-value
Δw	Maximum differential settlement

References

Bentley. (2022). *PLAXIS 3D manuals.* Delft, The Netherlands.

Cong, H.V., Takeuchi, K., Vakilazad, A., & Matsumoto, T. (2022). Parametric numerical study on deformation of the Tender Net Foundation subjected to vertical loading. In *Proceedings of the 11th International Conference on Stress Wave Theory and Design and Testing Methods for Deep Foundations* (6 p.), Rotterdam, The Netherlands. http://doi.org/10.5281/zenodo.7142087.

Dafalias, Y.F., & Manzari, M.T. (2004). Simple plasticity sand model accounting for fabric change effects. *Journal of Engineering Mechanics*, 130(6), 622-634. http://doi.org/10.1061/(ASCE)0733-9399(2004)130:6(622).

Japan Meteorological Agency – JMA. (2023). Retrieved in January 28, 2025, from https://www.jma.go.jp/jma/en/Activities/inttable.html.

Japan Road Association. (2012). *Specifications for highway bridges V: Seismic design.* Tokyo, Japan (in Japanese).

Kyoshin Network. (2022). *K-NET strong-motion seismograph network.* Retrieved in January 28, 2025, from https://www.kyoshin.bosai.go.jp/.

Nakai, T., Shahin, H.M., Kikumoto, M., Kyokawa, H., Zhang, F., & Farias, M.M. (2011). A simple and unified three-dimensional model to describe various characteristics of soils. *Soil and Foundation*, 51(6), 1149-1168. http://doi.org/10.3208/sandf.51.1149.

Takeuchi Construction Inc. (2025). Retrieved in January 28, 2025, from https://www.takeuchi-const.co.jp/en/.

The Building Center of Japan. (2019). *Recommendations for design of building foundations.* Tokyo, Japan (in Japanese).

Tokimatsu, K., & Yoshimi, Y. (1983). Empirical correlation of soil liquefaction based on SPT *N*-value and fines content. *Soil and Foundation*, 23(4), 56-74. http://doi.org/10.3208/sandf1972.23.4_56.